Green Chemistry

PAPER

View Article Online
View Journal | View Issue

Cite this: *Green Chem.*, 2014, **16**, 761

Tungsten carbides as selective deoxygenation catalysts: experimental and computational studies of converting C3 oxygenates to propene

Hui Ren,[a] Ying Chen,[a] Yulin Huang,[a] Weihua Deng,[a] Dionisios G. Vlachos[a] and Jingguang G. Chen*[b]

Received 28th June 2013,
Accepted 22nd August 2013

DOI: 10.1039/c3gc41256c

www.rsc.org/greenchem

The deoxygenation activity and selectivity of tungsten monocarbide (WC) have been investigated using a combination of DFT calculations, surface science experiments, and reactor evaluations of catalyst particles. Both WC surfaces and particles are very selective in breaking the C–O/C=O bond of propanol and propanal, leading to the production of propene as the main product. The consistency of DFT, surface science and reactor studies in predicting the high selectivity in C–O/C=O scission suggests that fundamental studies on model surfaces can be extended to more practical applications. Results from the current paper also identify research opportunities in synthesizing nanoparticle WC and W_2C as effective deoxygenation catalysts.

1. Introduction

The production of fuels and chemicals from renewable biomass resources is a promising approach to meet some of the energy and environmental challenges.[1–3] However, the derivatives of biomass, such as sugars and polyols, are over functionalized with a large number of oxygen atoms per molecule,[4,5] which need to be removed *via* selective deoxygenation to produce more valuable fuels and chemicals.[6]

For example, biodiesel is one of the most important biomass-derived biofuels as a replacement of a blending agent to petroleum diesel. However, the oxygen content leads to higher density and polarity,[4] resulting in higher viscosity and lower cold flow properties compared to conventional diesel.[7] Furthermore, the presence of oxygen also reduces the energy density of the fuel.[4,8–10] If biomass-derived fuels can be selectively deoxygenated, biodiesel can potentially be used as a direct replacement of conventional petroleum resources.[11]

Deoxygenation can proceed *via* either decarbonylation or selective C–O bond cleavage.[4,5] The former route often leads to the reduction in carbon chain length, which is often undesirable for conversion to fuels and chemicals;[4] moreover, the CO_2 produced from this route is not environmental friendly.[12] Therefore, selective deoxygenation *via* C–O bond cleavage is crucial in converting biomass derivatives to fuels and chemicals without reducing the number of carbon atoms. A good catalyst for deoxygenation should be active enough to cleave the C–O bond while remaining relatively inert toward C–C bond cleavage. In the current study, we use propanol and propanal as probe molecules to demonstrate that tungsten monocarbide (WC) is a promising catalyst for the selective scission of the C–O and C=O bonds. The reactions of propanol have been reported on several transition metals[13,14] and bimetallic systems.[15–20] To the best of our knowledge, none of these materials are selective toward deoxygenation without breaking some of the C–C bonds.

Transition metal carbides, in particular, tungsten and molybdenum carbides, have been evaluated for applications in both heterogeneous catalysis[21,22] and electrocatalysis.[22,23] Although these materials often show "platinum-like" properties in hydrocarbon transformation reactions,[21,22] recent studies reveal that for the reactions of oxygenate molecules, carbides are often different from either their parent metals or platinum.[24,25] Of particular relevance to deoxygenation is the reaction of methanol and ethanol on the WC surface, which shows that the WC surface is active towards C–O bond cleavage.[24,25] More recently, it is also reported that these carbides are active in deoxygenation reactions.[26–30]

In the current study, we use a combination of density functional theory (DFT) calculations, surface science experiments, and reactor studies to investigate the deoxygenation reactions of propanol and propanal on WC, which demonstrates as a case study starting from fundamental theoretical studies and then extending to more practical catalysis applications. The mechanistic insights into the deoxygenation pathways and the

[a]*Catalysis Center for Energy Innovation, University of Delaware, Newark, DE 19716, USA*
[b]*Department of Chemical Engineering, Columbia University, New York, NY 10027, USA. E-mail: jgchen@columbia.edu*

excellent selectivity of WC are predicted from DFT calculations; the deoxygenation reactions on model WC surfaces are verified by temperature programmed desorption (TPD) and the additional information of surface reaction intermediates is provided by surface vibrational spectroscopy; the selective deoxygenation over WC particles is then demonstrated by reactor studies. The selection of C3 oxygenates is mainly due to their relatively high vapor pressure, which allows one to introduce them into ultrahigh vacuum (UHV) systems for fundamental surface science studies and for gas-phase reactor evaluations. The comparison of propanol and propanal provides useful information on whether and how the deoxygenation activity differs between C–O and C═O bonds, which often coexist in biomass derived molecules.

2. Methods

2.1. DFT methods

The DFT calculations were performed using the SIESTA program.[31] The pseudo-potentials were generated using the Troullier–Martins scheme.[32] For W, the electrons of $6s^2$ and $5d^4$ were included as valence electrons. For all of the atoms, a double zeta with polarization quality basis set was employed. The exchange-correlation energy was determined using the generalized gradient approximation (GGA) functional proposed by Perdew, Burke, and Ernzerhof (PBE).[33] The localization radii of the basic functions were determined from an energy shift of 0.01 eV. In this work, the spacing of the grid points corresponded to an equivalent of 200 Ry energy cutoff in the associated reciprocal space at which value the geometries and energies have converged. Spin polarization was included whenever necessary. The calculated equilibrium lattice parameters for WC (hexagonal, $a = b = 2.92$ Å and $c = 2.85$ Å) are very similar to the experimental values ($a = b = 2.91$ Å and $c = 2.84$ Å).[34] The supercell approach was used to model the W-terminated WC(0001) surface (hereby referred to as WC(0001)); six layers of WC(0001) surface were modeled with 15 Å vacuum spacing between slabs. The bottom four layers of metal atoms were fixed at their bulk truncated position and the top two layers and the adsorbates were allowed to relax. A 3 × 3 unit cell was used in all the calculations and a Monkhorst–Pack mesh of 3 × 3 × 1 was employed in the *k*-point sampling. In this work, some of the structures and energetic results obtained from the SIESTA code were further checked using the pseudopotential plane-wave VASP code[35,36] (see Table 1). As can be seen from Table 1, the calculated results using SIESTA are very close to those from the VASP code.

2.2. Surface science studies

The preparation of the WC surface was described in detail elsewhere.[37] Briefly, the WC surface was prepared by carburizing a polycrystalline W foil using cycles of ethylene sputtering at 300 K, followed by annealing the surface to 1200 K. The stoichiometry of the W : C ratio was around 1 : 1, as confirmed by the Auger Electron Spectroscopy (AES), and was consistent with previous studies of the characterization of W terminated WC(0001).[38]

Table 1 Calculated chemisorption energies of $CH_3CH_2CH_2OH$, $CH_3CH_2CH_2O$, and CH_3CH_2CHO and enthalpy changes (ΔH) of some key reactions on WC(0001) using SIESTA and VASP codes

	E_{ad} and ΔH (eV)	
Species and reactions	VASP code	SIESTA code
$CH_3CH_2CH_2OH$	0.69	1.04
$CH_3CH_2CH_2O$	4.05	4.11
CH_3CH_2CHO	1.69	2.04
$CH_3CH_2CH_2OH \rightarrow CH_3CH_2CH_2O + H$	−1.77	−1.84
$CH_3CH_2CHO \rightarrow CH_3CH_2CH + O$	−2.39	−2.42

The exposure of propanol and propanal was achieved through leak valves. The samples were purified by successive freeze–pump–thaw cycles before use. The TPD measurements were taken from 105 K to 800 K with a linear heating rate of 3 K s^{-1}.

High-resolution electron energy loss spectroscopy (HREELS) measurements were recorded with the angles of incidence and reflection at 60 degrees with respect to the surface normal in the specular direction and with a primary beam energy of 6 eV. After the adsorption of propanol or propanal at 100 K, the surface was flashed to the next temperature of interest and allowed to cool back to 100 K before proceeding with the subsequent scan.

2.3. Synthesis and characterization of WC catalyst particles

The synthesis of WC particles was conducted in a sealed quartz tube reactor using ammonium metatungstate hydrate ($(NH_4)_6H_2W_{12}O_{40}$, Sigma-Aldrich) as tungsten precursor and cetyltrimethylammonium bromide (CTAB, Sigma-Aldrich) as the carbon source. Typically, 0.297 g of $(NH_4)_6H_2W_{12}O_{40}$ was mixed with 0.112 g of CTAB and placed in the bottom of the quartz tube. The quartz tube was then sealed under high vacuum before it was placed in an electrical resistance furnace to be carburized. The sample in the quartz tube was heated to 1273 K from room temperature with a heating rate of 1 K per minute. It was naturally cooled to room temperature after being held at 1273 K for one hour. The black powder at the bottom of quartz tube was collected.

Powder X-ray diffraction patterns (XRD) were obtained using a Phillips Norelco powder diffractometer using Cu Kα irradiation to examine the purity of the WC catalyst. Particle morphology was measured using a JOEL JEM-2010F transmission electron microscope (TEM) with a 200 kV acceleration voltage.

2.4. Reactor studies

The vapor phase deoxygenation of propanol/propanal, both with and without hydrogen, was carried out by flow reactor studies in a quartz glass reactor under atmospheric pressure at 653 K. Prior to reaction, the WC catalyst (0.043 g) was reduced under a H_2 (25 mL per minute) and He (25 mL per minute)

mixture at 723 K for 1 hour. During the reaction, a constant flow of propanol/propanal was obtained by bubbling He through a saturator containing propanol/propanal. In the experiments with co-feed H_2, the molar ratio of H_2 to propanol/propanal was calculated to be 10 : 1. The products were analyzed using an online GC (Agilent 7890A) equipped with a flame ionization detector (FID) and a thermal conductivity detector (TCD).

3. Results and discussion

3.1. DFT calculations

DFT calculations were performed to explore the decomposition pathways of propanol and propanal on WC(0001). The reaction network and the energy profile for propanol decomposition on WC(0001) are presented in Fig. 1. Fig. 1(a) shows that the chemisorption energy of propanol is 1.05 eV. The initial decomposition of adsorbed propanol on WC(0001) *via* O–H bond scission (a reaction barrier of E_a = 0.66 eV) is kinetically favorable over C–H bond scission (E_a = 1.50 eV), which is consistent with previous DFT results for methanol on WC(0001).[39] Based on the activation barriers, DFT results show that the propoxy ($CH_3CH_2CH_2O$) intermediate prefers to be further dehydrogenated to CH_3CH_2CHO rather than being dissociated into $CH_3CH_2CH_2$ and O. Propanal adsorbs on the surface through O to the bridge site and C to the top site, with a binding energy of 2.04 eV. A relatively low activation barrier (E_a = 0.33 eV) is obtained for the C=O bond scission of propanal on WC(0001). As shown in Fig. 1(b), the overall reaction is highly exothermic (ΔH = −4.40 eV), indicating that this reaction pathway for propanol decomposition is, aside from kinetic considerations, also thermodynamically favored. The decomposition of propanol goes through two elementary dehydrogenation steps to form the key intermediate (CH_3CH_2CHO) rather than having the C–O bond breaking first. Once CH_3CH_2CHO forms, C=O bond breaking occurs readily to produce CH_3CH_2CH, as shown in Fig. 1(a). The reaction network suggests that propanol and propanal share very similar deoxygenation intermediate and pathway, which are further confirmed in surface science studies as described below. Other dehydrogenation and C–C bond scission pathways show higher activation barriers, as illustrated in Fig. 1(a). As the deoxygenation product is CH_3CH_2CH, which has a very similar formula and structure with propene, it is a reasonable prediction that propene would be the main product of the deoxygenation reaction.

In summary, DFT calculations predict that the WC(0001) surface should exhibit high activity towards selective C–O/C=O bond scission of propanol and propanal to produce propene, and adsorbed CH_3CH_2CHO is the key intermediate that undergoes C=O bond cleavage with a low activation barrier of 0.33 eV. It should be pointed out that the current study used the closed-packed WC(0001) surface to obtain activation barriers and reaction networks. Additional calculations on the more open surface structures should provide additional insight into correlating model surfaces with polycrystalline or amorphous WC catalysts.

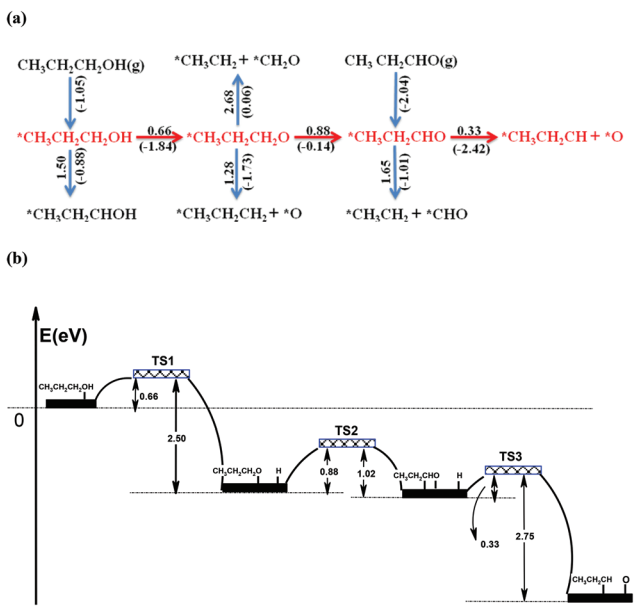

Fig. 1 (a) Schematic of the possible reaction pathway for propanol and propanal decomposition on the WC(0001) surface. The activation barrier (and the corresponding reaction energy in parenthesis) is in eV. The energetically favorable pathway is highlighted in red. (b) Energy profile of the most favorable reaction pathway for propanol decomposition on the WC(0001) surface.

3.2. Surface science studies

The TPD results following the adsorption of propanol on the WC surface at ~100 K are shown in Fig. 2, with Ni-modified WC also shown as reference to show the different reaction pathways of propanol on the two surfaces. As predicted in the reaction network in Fig. 1, selective C–O bond scission should lead to the formation of the CH_3CH_2CH intermediate, which can undergo isomerization to produce propene. In contrast, the C–C bond scission of propanol should lead to the formation of CO, C2 or C1 oxygenates and C2 or C1 hydrocarbons. As shown in Fig. 2, a broad desorption peak of propene (C_3H_6, 42 amu) is observed at 409 K, indicating the cleavage of the C–O bond. Relatively weak peaks are also detected in the 28 and 27 amu spectra on the WC surface, which are due to either the cracking fragments from propene or trace amount of ethylene. Because the 27 amu and 28 amu peaks are most likely from the cracking patterns of propene, the TPD results also suggest that CO (28 amu) is not produced. The absence of the 15 amu and 16 amu peaks suggests that there is no methane generated on the surface. The TPD results reveal that propene is the dominant reaction product from WC, indicating the selective deoxygenation pathway on the WC surface, which is also consistent with the DFT prediction. In comparison, on the Ni-modified WC surface, propene is not produced. Instead ethylene (C_2H_4, 27 amu) and CO (28 amu) are the main products from the decomposition of propanol, demonstrating that C–C bond cleavage is the main reaction

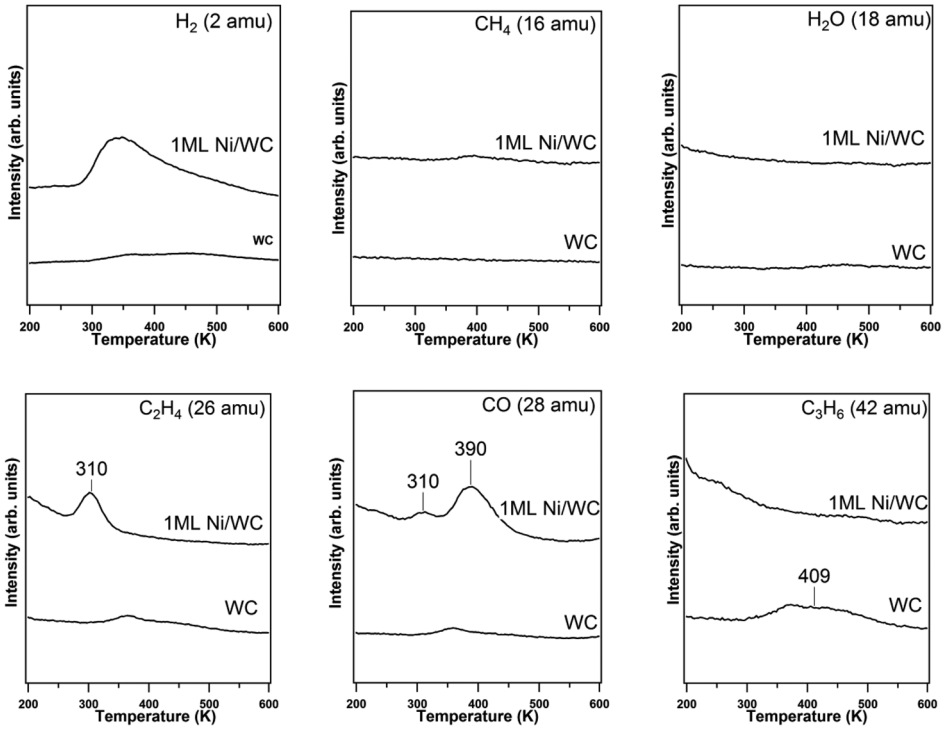

Fig. 2 TPD results following the decomposition of propanol on WC. Similar TPD spectra are also included for a Ni-modified WC surface to provide a reference of mass spectrometry sensitivity for different masses and to highlight the unique gas-phase product distribution from the WC surface.

pathway on the Ni/WC surface. In summary, the reactions of propanol decomposition on WC are as follows:

(a) $C_2H_5CH_2OH \rightarrow C_3H_6 + H_2 + O_{(ads)}$ deoxygenation
(b) $C_2H_5CH_2OH \rightarrow 3C_{(ads)} + O_{(ads)} + 4H_2$ total decomposition

Integrating the peak areas of the reaction products allows for quantification of activity for each decomposition reaction pathway. The yield of H_2 was determined by converting the H_2 TPD peak area to H_2 coverage based on the calibration of mass spectrometer saturation coverage using a Pt(111) surface.[40,41] The yield of C_3H_6 was determined by using an experimentally determined sensitive factor relative to CO, which was obtained by back filling the UHV system with equal concentrations of C_3H_6 and CO based on the ionization sensitivity factors of these molecules. The quantification of TPD peak areas indicates that the amount of propanol undergoing deoxygenation and total decomposition is 0.061 and 0.002 molecule per surface W atom, respectively, as summarized in Table 2.

In order to investigate whether WC is also active toward breaking the C=O double bond, as predicted by DFT calculations, propanal TPD experiments were performed. As shown in the TPD results in Fig. 3, similar to propanol, propene is again observed as the only hydrocarbon product from the WC surface, indicating that WC is similarly active to C=O bond cleavage without breaking the C–C bond, consistent with the DFT prediction. The quantified yield of the amount of propanal undergoing deoxygenation and total decomposition is 0.091 and 0.001 molecule per surface W atom, respectively. In comparison, on the Ni/WC surface, propanal primarily undergoes C–C bond cleavage to produce ethylene and CO, which is consistent with the previous study on a Ni(111) film.[15]

The unique selectivity of WC toward C–O or C=O bond scission can be explained by the fact that oxygenates are absorbed onto the WC surface *via* strong bonding through the oxygen atom.[24,42] The similarities between propanol and propanal in the TPD experiments suggest that these two

Table 2 Quantification of TPD results of propanol and propanal through different reaction pathways on WC surfaces: (a) deoxygenation[a], (b) total decomposition[b], (c) reforming[c] and (d) methane formation[d]

	Propanol					Propanal				
Surface	*a*	*b*	*c*	*d*	Total	*a*	*b*	*c*	*d*	Total
WC	0.061	0	0.000	0.002	0.063	0.091	0	0.000	0.001	0.092
1ML Ni/WC	0.000	0.018	0.095	0.062	0.175	0.000	0.015	0.093	0.057	0.165

[a] $C_2H_5CH_2OH \rightarrow C_3H_6 + H_2 + O_{(ads)}$; $C_2H_5CHO \rightarrow C_3H_6 + O_{(ads)}$. [b] $C_2H_5CH_2OH \rightarrow 3C_{(ads)} + O_{(ads)} + 4H_2$; $C_2H_5CHO \rightarrow 3C_{(ads)} + O_{(ads)} + 3H_2$. [c] $C_2H_5CH_2OH \rightarrow CO + 4H_2 + 2C_{(ads)}$; $C_2H_5CHO \rightarrow CO + 3H_2 + 2C_{(ads)}$. [d] $C_2H_5CH_2OH \rightarrow 2CH_4 + CO$; $C_2H_5CHO \rightarrow CH_4 + 2C_{(ads)} + O_{(ads)} + H_2$.

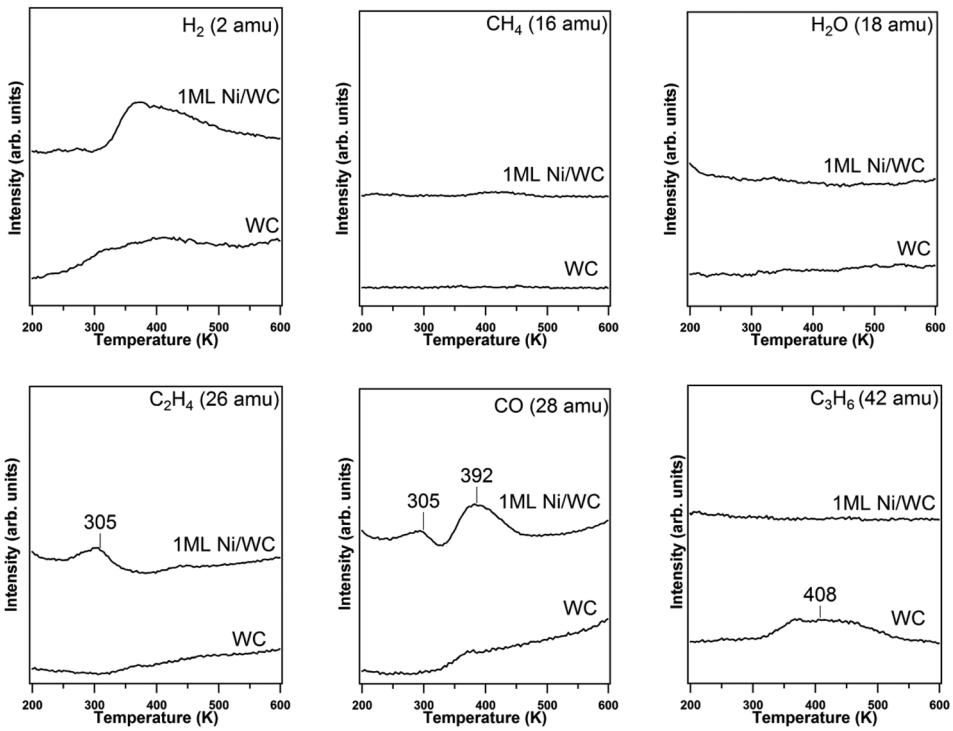

Fig. 3 TPD results following the decomposition of propanal on WC. Similar TPD spectra are also included for a Ni-modified WC surface to provide a reference of mass spectrometry sensitivity for different masses and to highlight the unique gas-phase product distribution from the WC surface.

molecules may have similar decomposition pathways on the WC surface. HREELS experiments were performed to determine the surface reaction intermediates from the decomposition of propanol and propanal. Fig. 4 compares the HREELS results after the adsorption at 100 K and after heating to 300 K, which is below the onset temperature for the desorption of the propene product.

As summarized in the vibrational assignment in Table 3, the spectrum following the adsorption of propanal at 100 K is characteristic of molecularly adsorbed propanal. Upon heating to 300 K, the intensity of the (C═O) mode at 1670 cm^{-1} significantly decreases, indicating that the bonding of propanal on WC occurs through the formation of the di-σ C–O bond. In comparison, the adsorption of propanol on WC leads to the dissociation of the O–H bond at 100 K, as indicated by the absence of the (O–H) mode, expected at 3687 cm^{-1} for gas-phase propanol and typically observed at above 3300 cm^{-1} for hydrogen-bonded alcohols. This observation is consistent with the previous studies of methanol and ethanol decomposition on WC, where dissociation of the O–H bond also occurs at 100 K.[24,25,42] This observation is also consistent with the DFT calculations of the initial decomposition of propanol on WC (Fig. 1). As compared in Table 3, the frequencies of all other vibrational features remain similar to those of propanol, indicating that the propoxy species is produced on WC at 100 K. Furthermore, the general similarity between the 300 K spectra of propanol and propanal suggests that a similar surface intermediate is produced, most likely a propoxy ($CH_3CH_2CH_2$–OW) and a di-σ bonded propanal (CH_3CH_2CHW–OW), respectively.

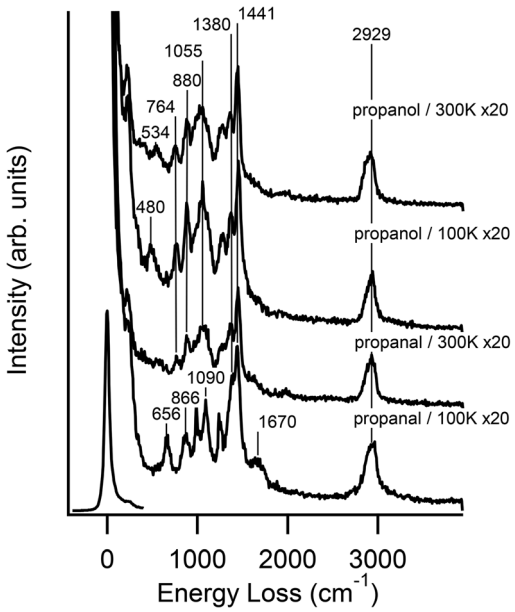

Fig. 4 HREELS spectra from exposure of the WC surface to propanol or propanal.

The similar nature of the two surface species is consistent with the similar TPD peak shape of propene from both molecules (Fig. 2 and 3).

Summarizing the results on the WC surface, DFT calculations predict that WC exhibits high activity towards selective C–O/C═O bond scission to produce propene, which is further

Table 3 Vibrational assignment for adsorbed propanal and propanol

Propanal			Propanol		
	Frequency (cm^{-1})			Frequency (cm^{-1})	
Mode	Liquid	WC	Mode	Gas	WC
$\nu(CH_3)$	2966	2929	$\nu(OH)$	3687	—
$\nu(CH_3)$	2909	2929	$\nu_a(CH_3)$	2978	2929
$\nu(CO)\eta^1$-EtCHO	1730	1670	$\nu_s(CH_3)$, $\nu_s(CH_2)$	2892	2929
$\delta(CH_2)$	1458	1441	$\delta(CH_2)$	1464	1441
$\delta(CH_3)$	1418	1380	$\delta(CH_3)$	1464, 1393	1380
$\nu_a(CCC)$	1092, 1120	1090	$\rho(CH_2)$	1393, 1300	n.r.
$\rho(CH_3)$	898	866	$\delta(COH)$	1218	—
$\delta(CCO)$	660	656	$\rho(CH_3)$	1063, 898	1055
			$\nu_a(CCO)$	1047, 971	1055
			$\nu_s(CCO)$	898	880
			$\gamma(CH_2)$	685	n.r.
			$\delta(CCC)$	463	480
			$\delta(CCO)$	463	480

confirmed by the TPD experiments. DFT calculations also suggest that propanol and propanal have a similar reaction intermediate, and undergo similar decomposition pathway on WC surface, which is verified by the HREELS measurements. Both computational and experimental results show that the WC surface is highly selective to C–O/C═O bond cleavage, suggesting that WC may be potentially used as a selective deoxygenation catalyst, as verified below.

3.3. Characterization and reactor studies of WC catalysts

In order to extend model surfaces to catalyst particles, WC catalyst was synthesized and tested in a flow reactor. The XRD pattern in Fig. 5(a) shows that the catalyst particle can be indexed to a hexagonal WC phase.[43] The 2θ of 31.54, 34.84, 48.48, 64.16, 64.58, 73.28, 75.62 and 75.86° corresponds to (001), (100), (101), (110), (002), (111), (200) and (102) facets of WC, respectively. The TEM images of the WC catalyst are shown in Fig. 5(b). The high resolution TEM micrograph in Fig. 5(c) clearly indicates that the WC particle is highly crystalline in nature with lattice fringes with d spacing of 0.2942, 0.2452 and 0.1981 nm, which closely matches the (001), (100) and (101) planes of hexagonal WC.[43,44] The average size of the catalyst particle is around 100 nm from Fig. 5(b). The large particle size is most likely related to the high synthesis temperature (1273 K in the current study) that is required to achieve the WC phase.

The results of reactor evaluation of propanol deoxygenation are shown in Fig. 6. Fig. 6 reveals that C3 hydrocarbons (mainly propene) and propanal are the main gas products, with trace amounts of C2 hydrocarbons, CO, CH_4 and C_6 hydrocarbons. The high selectivity (>95%) of C3 hydrocarbons suggests that deoxygenation is the dominant reaction with little C–C bond scission, which is consistent with the DFT calculations and surface science results. Due to the low steady-state conversion over the WC catalysts, it is difficult to determine the exact role of H_2 in the current study. However, results from previous studies of C3 oxygenates over Mo_2C catalysts,

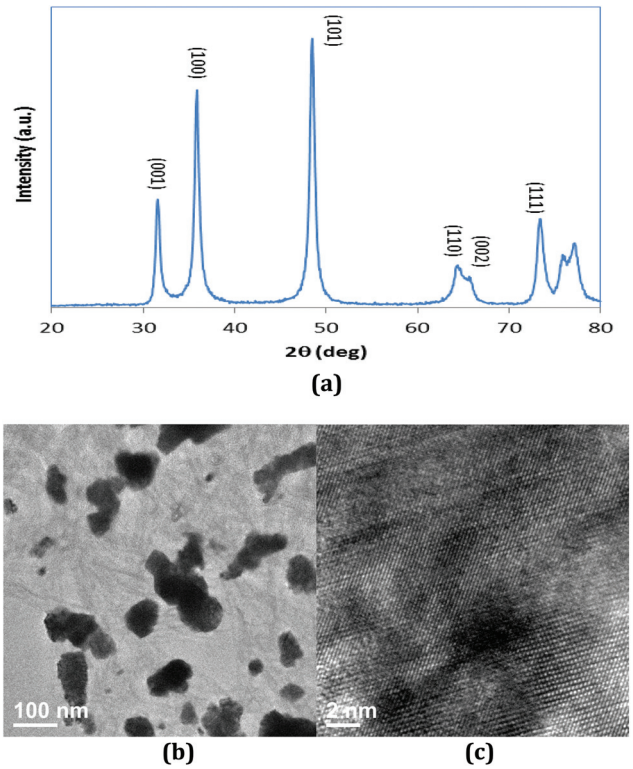

Fig. 5 Characterizations of powder WC: (a) XRD; (b) TEM; (c) HRTEM.

with a high steady-state conversion, clearly indicated that co-feeding H_2 led to the production of H_2O by removing the surface oxygen from the carbide catalysts.[29]

The results of propanal deoxygenation are shown in Fig. 7. The product distribution is more complicated in the case of propanal compared to that of propanol. As reported before, propanal can undergo ketonization and condensation reactions on transition metal oxide catalysts,[45,46] a similar situation is also observed on WC. Apart from higher ketones and aldehydes, C6 hydrocarbons, produced from the coupling reactions of C3, are also detected in the products. Although there are many side products observed from the reaction, the highest selectivity remains to be the selective deoxygenation of propanal to produce C3 hydrocarbons (mainly propene), with only trace amounts of products from the C–C bond cleavage.

3.4. Insight from comparison of model surfaces and catalysts

Both DFT calculations and UHV experiments on WC surfaces predict that propanol and propanal should undergo selective C–O/C═O bond scission to produce propene. Such prediction is confirmed by the excellent selectivity to produce propene from the reactor evaluation of WC catalysts. These general similarities between model surfaces and catalyst particles illustrate the usefulness of combining theory and experiments in identifying catalytic materials.

On the other hand, there are two main inconsistencies between model surfaces and catalysts, which in turn provide

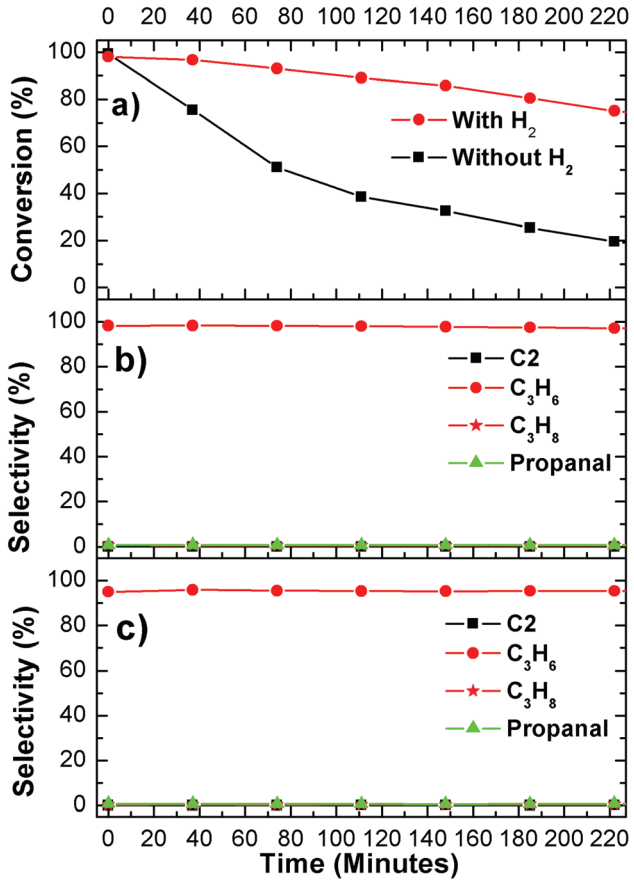

Fig. 6 Flow reactor results of propanol deoxygenation reactions at 653 K (reaction conditions: H_2–propanol = 10 : 1, catalyst 43.5 mg): (a) conversion; (b) selectivity with co-feed H_2; and (c) selectivity without co-feed H_2.

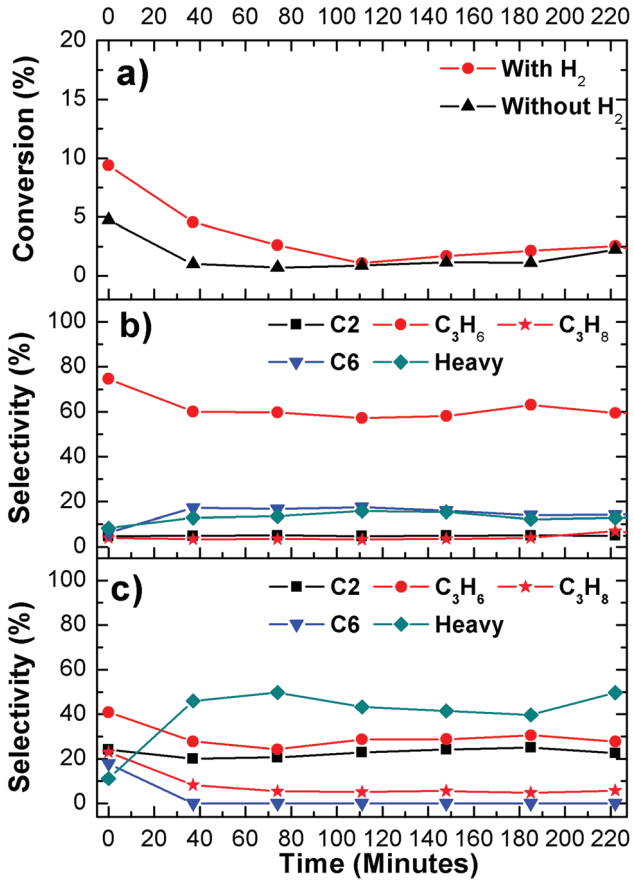

Fig. 7 Flow reactor results of propanal deoxygenation reactions at 653 K (reaction conditions: H_2–propanal = 10 : 1, catalyst 43.5 mg): (a) conversion; (b) selectivity with co-feed H_2; and (c) selectivity without co-feed H_2.

useful insight and future research opportunities in the utilization of WC catalysts for deoxygenation. The first is the difference between the deoxygenation activity of propanol and propanal. As suggested in DFT calculations (Fig. 1), propanol undergoes two elementary dehydrogenation steps to produce propanal before deoxygenation. This is consistent with the TPD measurements that the yield of propene is higher from the deoxygenation of propanal than from propanol on WC surfaces (Table 2). In contrast, in the reactor evaluation over WC catalyst the deoxygenation rate of propanal is significantly lower than propanol. One possible explanation is the presence of oxygen species over the WC catalyst, which is not present in the DFT and UHV studies of clean WC surfaces. The presence of oxygen on the WC catalyst should introduce acidic function from the oxidized W or WC, which should in turn enhance the dehydration pathway of propanol to directly produce propene. Further DFT and UHV studies on oxygen-modified WC surfaces are necessary to determine the role of surface oxygen in controlling the deoxygenation pathways.

The second inconsistency between model surfaces and catalysts is the very low steady-state conversion of propanal (Fig. 7 (a)). This is most likely due to the large size of the WC particles, ~100 nm, resulting from the high synthesis temperature (1273 K in the current study) that is required to achieve the WC phase. To highlight the importance of particle size, Fig. 8 compares the conversion and selectivity of propanal deoxygenation over WC and Mo_2C particles. The Mo_2C particle is in the range of 3 to 5 nm and correspondingly leads to a much higher steady-state conversion.[29] Interestingly, both WC and Mo_2C catalysts produce propene as the dominant product, suggesting similar deoxygenation pathways over the two carbide catalysts. The comparison in Fig. 8 suggests future opportunities in synthesizing and utilizing WC nanoparticles, preferably in the same particle range as that of Mo_2C, as effective deoxygenation catalysts. Another possibility is to utilize W_2C instead of WC, which should be easier to obtain in smaller particle size to the lower synthesis temperatures.

4. Conclusions

We explored the utilization of WC for the deoxygenation reactions of propanol and propanal using a combination of DFT calculations, UHV studies on model surfaces, and reactor evaluations of catalyst particles. These results demonstrate that WC is very selective in breaking the C–O/C=O bond. The

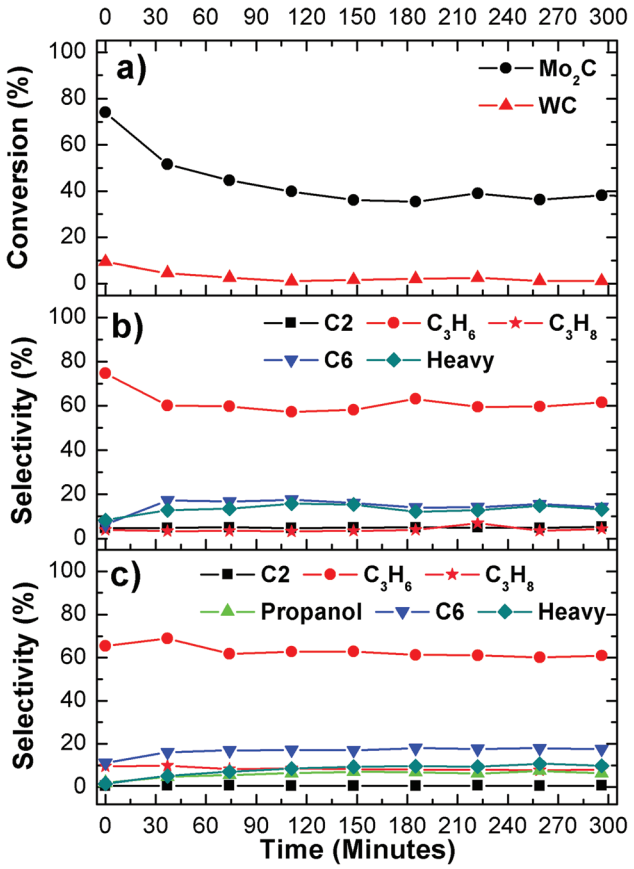

Fig. 8 Comparison of propanal with H_2 reactions on WC and Mo_2C: (a) conversion; (b) selectivity over WC; and (c) selectivity over Mo_2C.

dominant deoxygenation product is propene instead of propane; compared to saturated hydrocarbons, the advantages of producing unsaturated hydrocarbons are consuming less H_2 in the deoxygenation reaction and being more easily transformed into other value-added products. This unique property renders WC as a promising catalyst for the conversion of biomass-derived oxygenate molecules to fuels and chemicals. The consistency of DFT, surface science and reactor studies in predicting the high selectivity in C–O/C=O scission suggests a methodology that fundamental theoretical studies on model surfaces can be extended to more practical applications. Results from the current study also identify research opportunities in synthesizing nanoparticle WC and W_2C as effective deoxygenation catalysts.

Acknowledgements

This work was supported as part of the Catalysis Center for Energy Innovation, an Energy Frontier Research Center funded by the U.S. Department of Energy, Office of Basic Energy Sciences, Office of Science, under Award Number DE-SC0001004. We thank Dr Thomas Kelly for performing the HREELS measurements.

References

1 J. C. Serrano-Ruiz, R. M. West and J. A. Dumesic, *Annu. Rev. Chem. Biomol. Eng.*, 2010, **1**, 79–100.
2 T. V. Choudhary and C. B. Phillips, *Appl. Catal., A*, 2011, **397**, 1–12.
3 A. Corma, S. Iborra and A. Velty, *Chem. Rev.*, 2007, **107**, 2411–2502.
4 L. Petrus and M. A. Noordermeer, *Green Chem.*, 2006, **8**, 861–867.
5 J.-P. Lange, *Biofuels, Bioprod. Biorefin.*, 2007, **1**, 39–48.
6 R. A. Sheldon, *Catal. Today*, 2011, **167**, 3–13.
7 F. Jin, H. Zhong, J. Cao, J. Cao, K. Kawasaki, A. Kishita, T. Matsumoto, K. Tohji and H. Enomoto, *Bioresour. Technol.*, 2010, **101**, 7624–7634.
8 G. W. Huber, S. Iborra and A. Corma, *Chem. Rev.*, 2006, **106**, 4044–4098.
9 S. Czernik and A. V. Bridgwater, *Energy Fuels*, 2004, **18**, 590–598.
10 D. Mohan, C. U. Pittman and P. H. Steele, *Energy Fuels*, 2006, **20**, 848–889.
11 B. Smith, H. C. Greenwell and A. Whiting, *Energy Environ. Sci.*, 2009, **2**, 262–271.
12 W. Wang, S. Wang, X. Ma and J. Gong, *Chem. Soc. Rev.*, 2011, **40**, 3703–3727.
13 N. F. Brown and M. A. Barteau, *Langmuir*, 1992, **8**, 862–869.
14 J. L. Davis and M. A. Barteau, *Surf. Sci.*, 1990, **235**, 235–248.
15 L. E. Murillo and J. G. Chen, *Surf. Sci.*, 2008, **602**, 2412–2420.
16 D. A. Chen and C. M. Friend, *Langmuir*, 1998, **14**, 1451–1457.
17 T. Mongkhonsi, N. Chaiyasit and P. Praserthdam, *J. Chin. Inst. Chem. Eng.*, 2002, **33**, 365–372.
18 T. Mongkhonsi, P. Pimanmas and P. Praserthdam, *Chem. Lett.*, 2000, 968–969.
19 T. Mongkhonsi, W. Youngwanishsate, S. Kittikerdkulchai and P. Praserthdam, *J. Chin. Inst. Chem. Eng.*, 2001, **32**, 183–186.
20 I. A. Rodrigues, K. Bergamaski and F. C. Nart, *J. Electrochem. Soc.*, 2003, **150**, E89–E94.
21 *Chemistry of Transistion Metal Carbides and Nitrides*, ed. S. T. Oyama, Blackie, 1996.
22 H. H. Hwu and J. G. Chen, *Chem. Rev.*, 2005, **105**, 185–212.
23 E. C. Weigert, A. L. Stottlemyer, M. B. Zellner and J. G. Chen, *J. Phys. Chem. C*, 2007, **111**, 14617–14620.
24 H. Ren, D. A. Hansgen, A. L. Stottlemyer, T. G. Kelly and J. G. Chen, *ACS Catal.*, 2011, **1**, 390–398.
25 A. L. Stottlemyer, T. G. Kelly, Q. Meng and J. G. Chen, *Surf. Sci. Rep.*, 2012, **67**, 201–232.
26 J. Han, J. Duan, P. Chen, H. Lou, X. Zheng and H. Hong, *ChemSusChem*, 2012, **5**, 727–733.
27 J. Han, J. Duan, P. Chen, H. Lou and X. Zheng, *Adv. Synth. Catal.*, 2011, **353**, 2577–2583.
28 J. Han, J. Duan, P. Chen, H. Lou, X. Zheng and H. Hong, *Green Chem.*, 2011, **13**, 2561–2568.

29 H. Ren, W. Yu, M. Salciccioli, Y. Chen, Y. Huang, K. Xiong, D. G. Vlachos and J. G. Chen, *ChemSusChem*, 2013, **6**, 798–801.
30 R. W. Gosselink, D. R. Stellwagen and J. H. Bitter, *Angew. Chem., Int. Ed.*, 2013, **52**, 5089–5092.
31 J. M. Soler, E. Artacho, J. D. Gale, A. Garcia, J. Junquera, P. Ordejon and D. Sanchez-Portal, *J. Phys.: Condens. Matter*, 2002, **14**, 2745–2779.
32 N. Troullier and J. L. Martins, *Phys. Rev. B: Condens. Matter*, 1991, **43**, 8861–8869.
33 J. P. Perdew, K. Burke and M. Ernzerhof, *Phys. Rev. Lett.*, 1996, **77**, 3865–3868.
34 L. E. Toth, *Transition Metal Carbides and Nitrides*, Academic, New York, 1971.
35 G. Kresse and J. Hafner, *Phys. Rev. B: Condens. Matter*, 1994, **49**, 14251–14269.
36 G. Kresse and J. Furthmuller, *Comput. Mater. Sci.*, 1996, **6**, 15–50.
37 M. P. Humbert, C. A. Menning and J. G. Chen, *J. Catal.*, 2010, **271**, 132–139.
38 J. Brillo, A. Hammoudeh, H. Kuhlenbeck, N. Panagiotides, S. Schwegmann, H. Over and H. J. Freund, *J. Electron Spectrosc. Relat. Phenom.*, 1998, **96**, 53–60.
39 A. L. Stottlemyer, P. Liu and J. G. Chen, *J. Chem. Phys.*, 2010, **133**, 104702–104709.
40 P. R. Norton, J. A. Davies and T. E. Jackman, *Surf. Sci.*, 1982, **121**, 103–110.
41 G. Ertl, M. Neumann and K. M. Streit, *Surf. Sci.*, 1977, **64**, 393–410.
42 T. G. Kelly, A. L. Stottlemyer, H. Ren and J. G. Chen, *J. Phys. Chem. C*, 2011, **115**, 6644–6650.
43 F. P. Hu and P. K. Shen, *J. Power Sources*, 2007, **173**, 877–881.
44 S. Shanmugam, D. S. Jacob and A. Gedanken, *J. Phys. Chem. B*, 2005, **109**, 19056–19059.
45 M. Kobune, S. Sato and R. Takahashi, *J. Mol. Catal. A: Chem.*, 2008, **279**, 10–19.
46 A. Gangadharan, M. Shen, T. Sooknoi, D. E. Resasco and R. G. Mallinson, *Appl. Catal., A*, 2010, **385**, 80–91.